Scripta Materialia 171 (2019) 87–91

Contents lists available at ScienceDirect

Scripta Materialia

journal homepage: www.elsevier.com/locate/scriptamat

# Fabrication of artificial defects to study internal fatigue crack propagation in metals

Arnaud Junet[a,*], Alexandre Messager[b], Xavier Boulnat[a], Arnaud Weck[c,d,e], Elodie Boller[f], Lukas Helfen[f,g], Jean-Yves Buffiere[a]

[a] Université de Lyon, INSA-Lyon, MATEIS, CNRS UMR 5510, Villeurbanne F-69621, France
[b] Arts et Metiers ParisTech, I2 M Bordeaux, CNRS, Université de Bordeaux, Esplanade des Arts et Metiers, Talence F-33405, France
[c] Department of Mechanical Engineering, University of Ottawa, 150 Louis Pasteur, Ottawa, ON K1N 6N5, Canada
[d] Centre for Research in Photonics, University of Ottawa, 25 Templeton, Ottawa, ON K1N 6N5, Canada
[e] Department of Physics, University of Ottawa, 150 Louis-Pasteur, Ottawa, ON K1N 6N5, Canada
[f] ESRF, 71 avenue des Martyrs, BP 220, Grenoble Cedex 9 38043, France
[g] Institute for Photon Science and Synchrotron Radiation, Karlsruhe Institute of Technology, P.O. Box 3640, Karlsruhe D-76021, Germany

ARTICLE INFO

*Article history:*
Received 14 March 2019
Received in revised form 16 May 2019
Accepted 16 May 2019
Available online 30 June 2019

*Keywords:*
Internal fatigue cracks
Three-dimensional tomography
Synchrotron radiation
Titanium alloys
Spark plasma sintering

ABSTRACT

Fatigue specimens designed with controlled internal defects were obtained by diffusion bonding of Ti-6Al-4V sheets containing femtosecond laser drilled notches. Crack initiation from the internal defect occurred systematically. The cracks were characterised by *in situ* synchrotron X-ray tomography. Propagation rates are lower than those of surface cracks of comparable sizes in the same material and fall between experimental data obtained for fatigue cracks propagating in air and in vacuum.



The vast majority of failures of metallic industrial components are due to mechanical fatigue. Most of the time, fatigue crack initiation occurs at the surface of the metallic parts where plastic deformation is facilitated by lower constraint, plane stress, etc. However, in some cases – such as low applied stress (resulting in very long life times), parts with surface treatments inducing compressive residual stresses, large internal defects, etc. – an internal crack can initiate and lead to component failure. Several studies have been conducted to understand the mechanisms of the propagation of internal fatigue cracks [1]. Despite this relatively large amount of work, many questions remain unanswered such as the precise location of internal crack initiation, the relation between crack growth and the local microstructure, internal crack propagation rates, etc. Due to this lack of knowledge, the design of mechanical components can be very conservative. There are commonly two ways to study internal fatigue cracks. As the environment plays a key role on crack propagation rates [2], one can assume that internal cracks behave like surface cracks propagating in high (or ultra-high) vacuum. Thus, internal crack growth rates can be deduced from classical fatigue tests performed in controlled atmospheres such as vacuum, argon, etc. [3-7]. A critical issue with this approach is that the exact environment at the tip of a fatigue crack in a metal is not known and remains a topic for discussion in the literature [8]. The second method consists in studying *directly* internal cracks initiated from natural [8-11] or artificial [12] defects. Such measurements have to be made non-destructively and in the bulk of samples. In the gigacycle regime, some researchers have used frequency analysis during cycling and fracture surfaces to evaluate the number of cycles required for initiation and propagation [13]. This indirect method relies strongly, however, on the Paris law of the internal cracks which, as explained, is not known accurately. Recently, the growth rate of internal fatigue cracks has been reported for Ti and Al alloys [8-10]. The authors showed with synchrotron X-ray tomography that the internal crack growth rates are lower than those of surface cracks. The experimental data remain however limited as those experiments have to be carried out in a limited time (typically one to three days of beam

* Corresponding author.
*E-mail address:* arnaud.junet@insa-lyon.fr (A. Junet).

https://doi.org/10.1016/j.scriptamat.2019.05.018
1359-6462/ 

time) and are dependent on crack initiation on natural defects which, by essence, have scattered geometries and sizes.

To overcome those problems, we have developed a method described in this paper to produce artificial internal defects inside metallic tomography fatigue samples without altering the material microstructure. These defects lead systematically to internal crack initiation, which allowed to plot a first series of propagation curves that is discussed in this article.

The method described here (schematically summarized in Fig. 1) is inspired from the work of A. Weck et al. [14] who have used femtosecond laser machining to produce model materials in order to study monotonic fracture. The same type of machining was used in our study: shallow sharp notches were obtained at the surface of thin (~1 mm) sheets of commercially available Ti-6Al-4V alloy (ASTM F 136-13 standards). A Yb:KGW femtosecond laser (PHAROS from Light Conversion, Inc.) was used to generate linearly polarized laser pulses at a center wavelength of 1030 nm with pulse duration of 300 fs, and a repetition rate of 10 kHz. The laser beam was perpendicular to the sheets surfaces and focused using a 20× microscope objective in ambient atmosphere. The combination of a Glan polarizer and a half wave plate was employed to vary the laser power which was set at 100 mW. The sheets were mounted on a computer-controlled xyz translation stage (Aerotech ANT130XY-Z) and illuminated from the top to enable monitoring the laser micromachining process with a CCD camera. The laser ablation process was performed by translating the sheets relatively to the stationary laser beam in a back and forth motion (6 times) at the speed of 0.1 mm/s to create 200 µ m wide, 200 µ m deep and 20 µ m thick grooves. The sheets were then placed in an ultrasonic bath for 5 min to remove debris from the laser ablation process.

After mechanical polishing down to 1 µ m (diamond suspension) and ultrasonically cleaning up with acetone for 5 min, the notched sheet was diffusion bonded to another similarly polished sheet using a Spark Plasma Sintering (SPS) device HP D 25 of FCT Systeme Company. A load of 2 kN was applied by the punches on the two sheets put into contact. The chamber was evacuated and put under primary vacuum (PV) (~100 Pa) during the whole thermo-mechanical process. The applied load was adjusted to 37 kN resulting in a pressure of 15 MPa on the Ti-6Al-4V sheets. Then, the thermal cycle consisted in a heating rate of 100 °C/min up to the soaking temperature at 750 °C, a holding time of 10 min and finally a cooling stage at 20 °C/min down to 400 °C. Further, the sheets were naturally cooled down to room temperature. Fatigue specimens were machined around the drilled defects by Electrical Discharge Machining (EDM). The positioning of the notches in the sample gage length (±10 µ m) was ensured by X-ray radiography prior to EDM. Finally, the samples gage lengths were manually polished (2500 grit SiC paper) to obtain a circular cross-section of about 1 mm in diameter and avoid surface crack initiation at corners.

The grain structure of the SPS bonded material was characterised using Electron Back Scattered Diffraction (EBSD) in a scanning electron microscope (Zeiss Supra 55 VP with field-emission gun). Fig. 2 shows an Euler grain orientation map containing the Diffusion Bonding Interface (DBI). The microstructure is composed of the hcp alpha phase (surface fraction ~94%) with bcc beta phase at the grain boundaries. The average $\alpha$ grain diameter is 4.4 µm. The DBI is almost undetectable in secondary and backscattered electron modes; no voids nor intermetallic phases were found, indicating a very good joining of the two sheets. DB was carried out at a temperature lower than the Ti-6Al-4V $\beta$ transus (980 °C), so that the initial equiaxed alpha/beta duplex microstructure was retained, with no phase transformation upon cooling. Besides, the growth of alpha grains has been avoided by the high heating rate, the low holding temperature and short holding time during the SPS cycle.

This differs from the findings of Dong et al. [15], who observed a clear evolution of crystallographic texture in the alpha phase

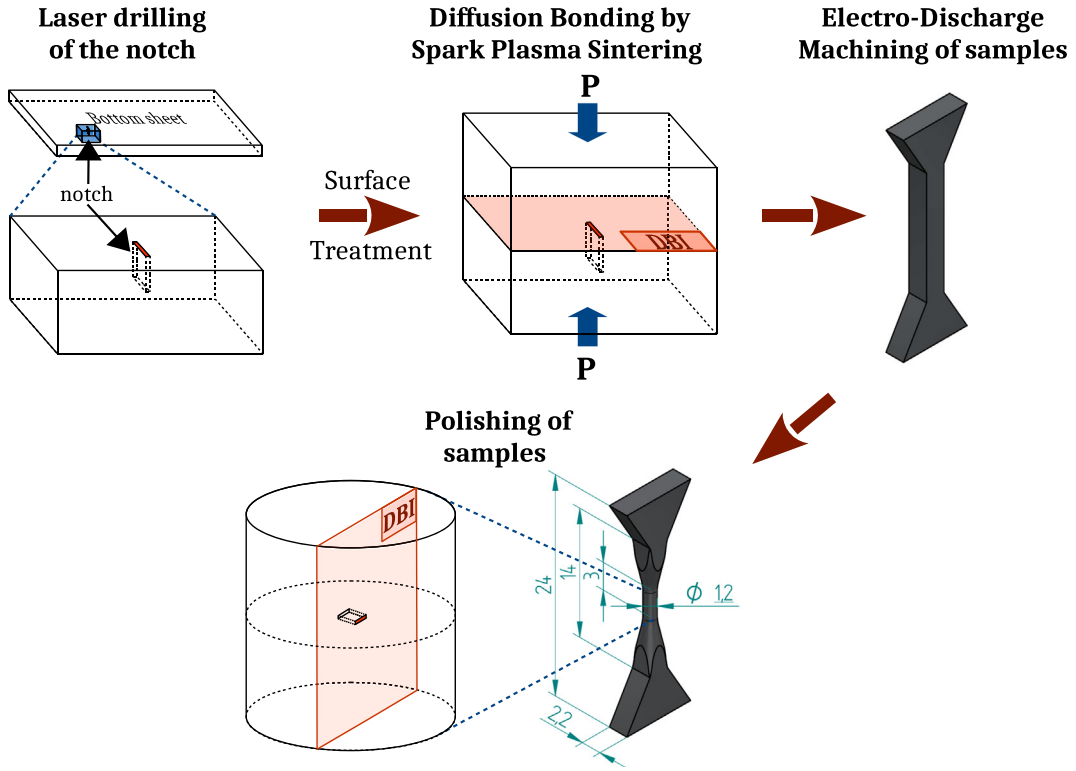


**Fig. 1.** Method of production of the fatigue specimens. The Diffusion Bonding Interface (DBI) is shown in orange.

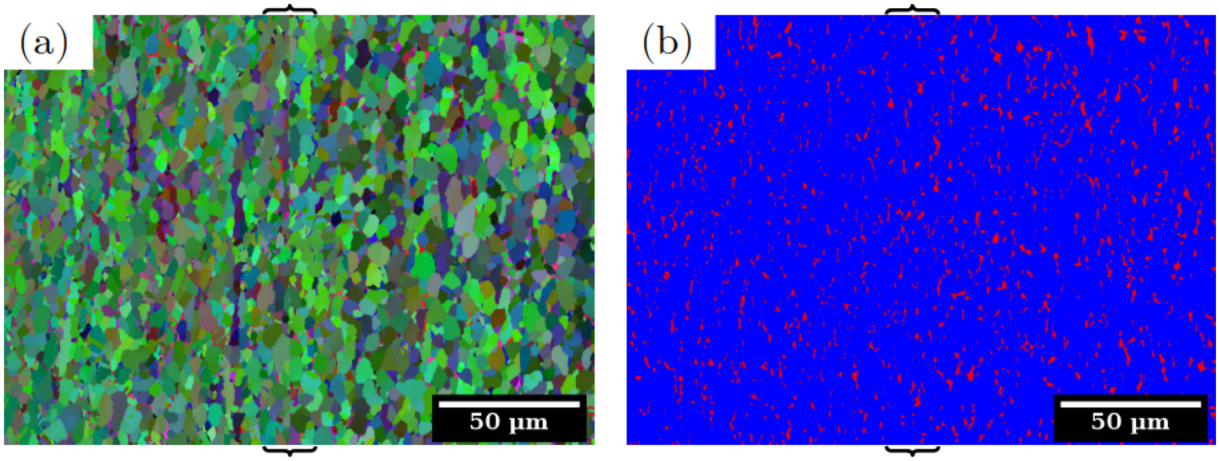


**Fig. 2.** (a) EBSD Euler map and (b) Phase map (alpha phase in blue and beta phase in red) of the alloy microstructure: the diffusion bonded interface (DBI) can hardly be detected (vertical region in the center of the black braces). Scan was performed at a magnification of ×500 with a step size of 200 nm.

between base material and interface after diffusion bonding at higher temperature (920 °C) for longer time (90 min). Some grains cross the interface, indicating the onset of recrystallization after efficient joining, as already observed by He al. [16] on a Ti-6Al-4V laminate also bonded by SPS at equivalent temperatures range.

A tensile test was carried out after the DB process with the stress axis contained within the DBI. The sample gage length was 15 mm and the applied strain rate was $2 \cdot 10^{-4}\,s^{-1}$. The tensile properties of the two sheets before and after DB are similar, which shows that the bonded material exhibits similar properties to those of the original material (Table 1).

Uniaxial fatigue tests (R = 0.1, f = 20 Hz) were performed *in situ* at the ESRF synchrotron facility on ID19 beamline using a fatigue device described in Ref. [17]. A maximum stress $\sigma_{max}$ between 400 and 520 MPa was used to ensure that, at the beginning of the test, the stress intensity factor (SIF) range ΔK was between the SIF threshold $\Delta K_{th\_air}$ for cracks growing in air and $\Delta K_{th\_vac}$ for cracks growing in vacuum [7, 18, 19] for Ti-6Al-4V with equivalent microstructure. During the tomographic scans, the sample was held in tension at $\sigma_{max}$ in order to hold the crack open and facilitate crack imaging. Images were captured using a pink beam at 60 keV with a CMOS PCO 5.5 detector (2048 × 2048 pixels). 2500 radiographs were acquired with an exposure time of 0.05 s and a voxel size of 0.72 µ m, leading to a scan duration of 3 min and a field of view of about 1.5 mm.

For on-line reconstruction and validation of the experiment, we used the tomographic algorithms described in Refs. [20] and [21]. After a first tomographic reference scan, the method used was as follows: (i) cycle the sample (ii) acquire a tomographic scan (iii) reconstruct a sub volume around the notch (iv) measure the crack size using a projected view along the stress direction (v) adjust the number of cycles taking into account the propagation rate, etc. After initiation, the cracks were observed to grow globally in mode I with a regular and almost circular shape (see Fig. 3 (a)); small reconstructed sub-volumes (typically 2048 × 2048 × 150 voxels) were sufficient to follow crack growth, allowing to analyze quantitatively crack growth nearly in real time. The six samples/propagation curves presented in this paper were obtained during four days of beamtime.

Fig. 3 (b) shows a typical fracture surface observed by scanning electron microscopy. The cracks systematically initiated at the artificial notch and propagated through the sample's bulk leading to its failure.

Crack initiation systematically occurred after a limited number of cycles (less than 5% of the specimens lifetimes). This study therefore focuses on the propagation of such cracks. From Fig. 3 (c), it can be seen that the cracks appear to be delayed at the DBI region (until ∼ half of the lifetime). A change in propagation rate was also observed by Dong et al. and explained by the variation in crystallographic microtexture around the DBI [15]; such a variation has not been observed in the present study. One explanation could be that the shape of the notch (wedge shape, see Fig. 3 (a)) tends to favor crack initiation away from the interface. To check this assumption, Finite Element calculations would be needed to examine the stress concentration factors/the SIF at the early stages of the propagation induced by this geometry. Even if the laser parameters could be optimized to produce a sharper notch with a smaller opening of the notch, this retardation effect is limited and the cracks quickly acquire a regular circular shape. At that stage, the crack length is more than 20 times larger than the grain size, therefore they can be considered as long cracks. Because of this circular shape, SIF calculations are more accurate than in the case of microstructurally short cracks with a complex shape such as in the work of Serrano et al. [10]. These cracks can therefore be compared with confidence with data from the literature obtained on macroscopic samples. At the end of the sample's lifetime, the growth rate of the part of the crack front closer to the sample surface appears higher than that of the other part of the front.

From the data of Fig. 3 (d) some $da/dN = f(\Delta K)$ curves can be derived (nominal ΔK values i.e. no closure correction). As in the work of Yoshinaka et al. [9] a global value of the crack size and of the SIF is computed using the $\sqrt{area}$ parameter introduced by Y. Murakami [22]. It can be seen from Fig. 3 (d) that the equivalent size of the crack $a_{eq}$[1]

$$a_{eq} = \sqrt{\frac{\text{area}}{\pi}} \tag{1}$$

**Table 1**
Tensile properties of Ti-6Al-4V sheets.

| Sheet | Tensile strength (MPa) | 0.2% proof stress (MPa) | Elongation (%) |
|---|---|---|---|
| Sheet 1 (containing the notch) | 1026 | 935 | 12 |
| Sheet 2 | 944 | 855 | 13 |
| DB sheets | 1070 | 915 | 14 |

[1] assuming the shape of a disk of radius $a_{eq}$.

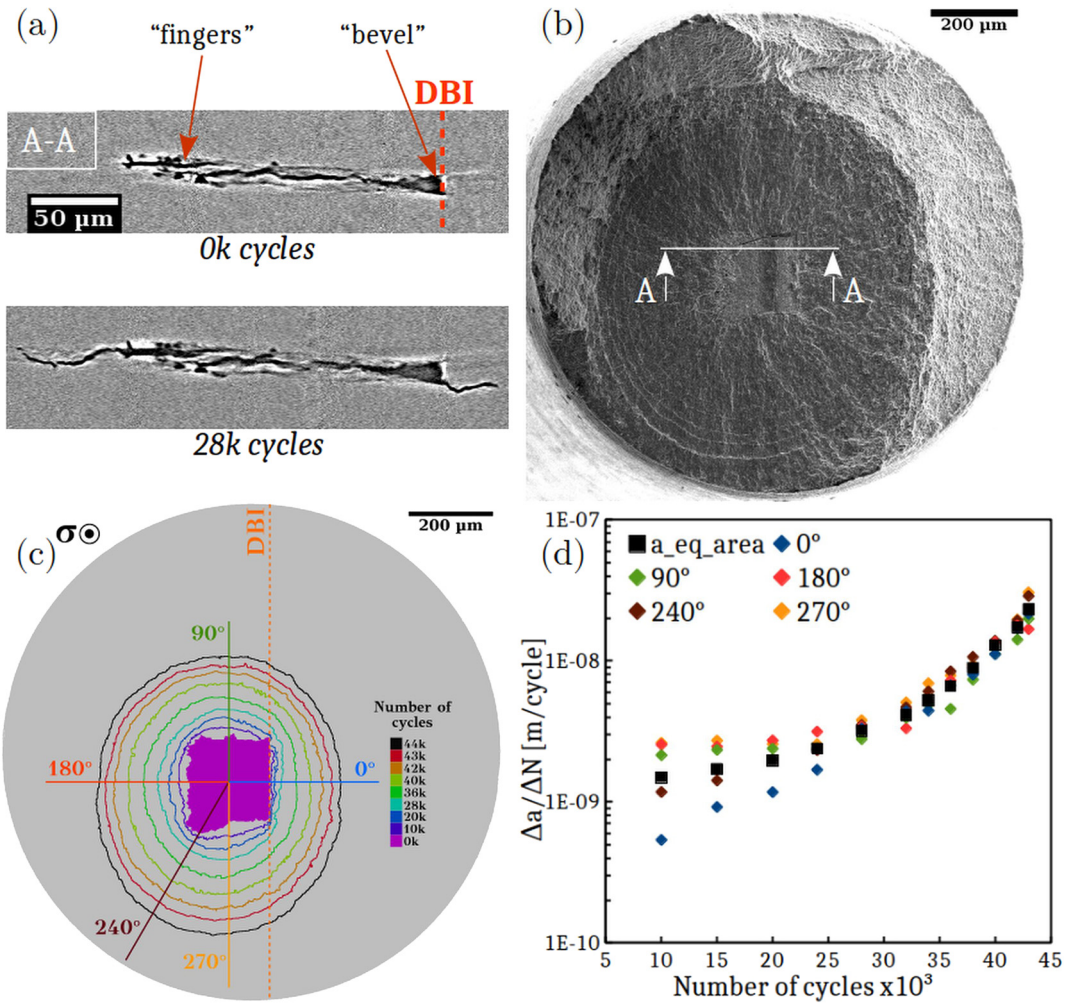


**Fig. 3.** (a) Sections views of the defect before and after fatigue testing. (b) Fractography of the A2_int specimen. (c) Projected views of the crack front at different stages of propagation. The Diffusion Bonding Interface is represented by an orange dotted line. (d) Crack growth rate over the number of cycles for different polar angles plotted in (c).

is a very good estimation of the average crack size. For ΔK, the following formula is used:

$$\Delta K = \kappa \sigma_{max}(1-R)\sqrt{\pi\sqrt{area}} \quad (2)$$

where $\kappa$ is equal to 0.5 for internal cracks and 0.65 for surface cracks, *area* is the projected area of the crack onto the plane perpendicular to the loading axis and *R* the stress ratio.

The resulting da/dN curves shown in Fig. 4 were obtained on six specimens as summarized in Table 2.

The data obtained for the surface crack are in good agreement with those obtained by Yoshinaka et al. [9] for the same material, giving us confidence in the ability of the *in situ* experiments to extract meaningful data in spite of the samples reduced size.

All the internal cracks obtained propagated at lower rates than those measured for surface cracks, which is consistent with previous studies [8-10]. As suggested by several authors for Ti [4] and Ti-6Al-4V alloy [3, 5-7], those lower crack growth rates can be linked to the crack tip environment i.e. a lower oxygen content than in air. Based on literature data on the kinetics of Ti alloys oxidation, the DB conditions (10 min holding time @ 750 °C) are such that the notch surface should oxidize and no more $O_2$ molecules should be present in the notch [23-25]. Hence, our da/dN data should superimpose on those obtained by Yoshinaka et al. for surface cracks growing in Ultra High Vacuum (UHV) or internal cracks [9].

Nevertheless, the literature data shows that even a very low partial pressure of oxygen can affect drastically the growth rate of a surface crack, and particularly in the near-threshold regime [6-8, 26]. For example, Oguma et al. [6] showed that for a similar Ti-6Al-4V alloy, a vacuum level variation from $2.7 \cdot 10^{-5}$ to $1.3 \cdot 10^{-1}$ Pa resulted in a variation in the crack propagation rate from $7.4 \cdot 10^{-11}$ to $1.0 \cdot 10^{-9}$ m/cycle for $\Delta K = 8$ MPa$\cdot$ m$^{1/2}$ (R = 0.1 – long crack regime – K decreasing). Yoshinaka et al. also found that – for the same $\Delta K$ – a vacuum level variation from $5 \cdot 10^{-6}$ to $\sim 10^{5}$ Pa resulted in a variation in the crack growth rate from $3.0 \cdot 10^{-11}$ to $5.0 \cdot 10^{-9}$ m/cycle (R = 0.1 — small crack regime). In addition, McClung et al. [27] discovered that a vacuum level lower than $1.33 \cdot 10^{-4}$ Pa was sufficient to remove environmental effects whereas Chapman et al. found that a vacuum of the order of $10^{-3}$–$10^{-4}$ Pa was not [8] (at elevated temperature). From these findings, one can assume that if vacuum levels inside the artificial notches should be better than the moderate vacuum of the SPS, it might not be as low as what can be assumed based on oxidation data. This hypothesis is in agreement with the fact that the argon specimens (C2 and C3) have the lowest values of da/dN for all the $\Delta K$ values investigated. The injection of this neutral gas probably evacuated more efficiently the oxygen molecules outside the notch and led to a lower partial pressure of oxygen before DB.

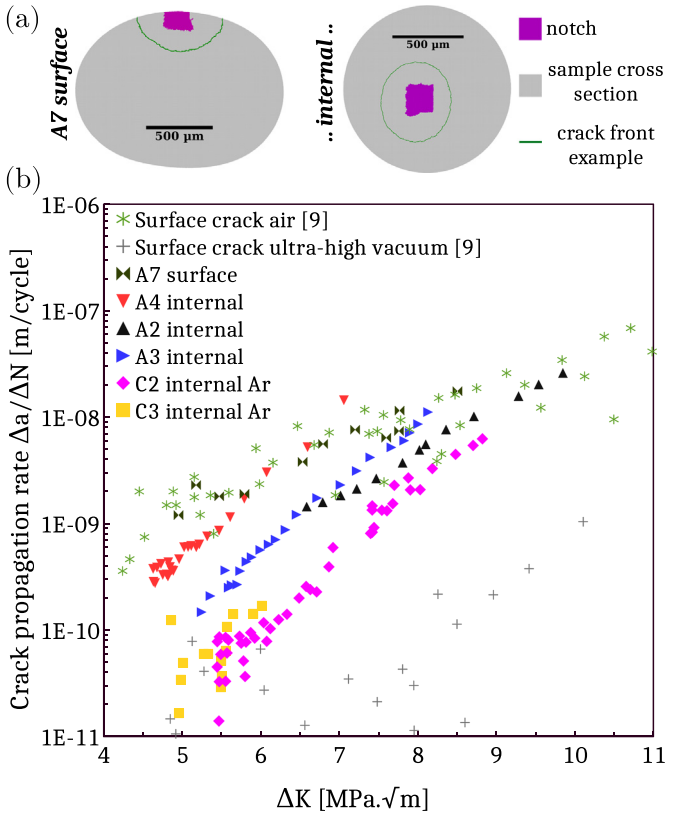


**Fig. 4.** (a) Samples sketches cross sections with the notch geometry for surface and internal crack monitoring. (b) da/dN curves of all the specimens tested compared to the literature data [9].

It could also explain the variability observed between samples (for samples A4 and A3 for example). Thermal treatments @ 750 °C and different holding times after SPS DB could be carried out to try to better control the environment inside the notch and further understand its influence on the fatigue lifetime.

To conclude, a novel method for characterising internal fatigue cracks has been successfully developed. Specimens with internal defects with a controlled shape were produced and efficiently tested *in situ* enabling the observation of internal cracks propagation. This method can potentially be extended to other metallic materials that can be joined by diffusion, such as steels and cast iron. Various shapes of internal defects could also be experimented to study the transient regime of internal propagation leading to a circular crack front.

This work was funded by the French National Research Agency (GIGADEF ANR project, grant number ANR-16-CE08-0039). We acknowledge the European Synchrotron Radiation Facility for provision of beamtime at beamline ID19. The authors express their gratitude to F. Mercier for his valuable assistance for SPS diffusion bonding.

**Table 2**
Summary of the in situ fatigue tests conditions and results.

| Specimen | SPS conditions | Maximum stress (MPa) | Fatigue life ($\times 10^3$ cycles) |
|---|---|---|---|
| A7 (surface) | Primary vacuum (PV) ~100 Pa | 320 | 87 |
| A4 (internal) | PV | 435 | 150 |
| A2 (internal) | PV | 530 | 45 |
| A3 (internal) | PV | 430 | 415 (Not broken) |
| C2 (internal Ar) | PV + Argon injection before DB (Ar ≥ 99.99%) | 455 | 718 (Not broken) |
| C3 (internal Ar) | PV + Argon injection before DB (Ar ≥ 99.99%) | 443 | 980 (Not broken) |

## References

[1] Y. Hong, C. Sun, Theor. Appl. Fract. Mech. 92 (2017) 331–350.
[2] G. Henaff, K. Marchal, J. Petit, Acta Metall. Mater. 43 (1995) 2931–2942.
[3] R.J.H. Wanhill, Metall. Trans. A 7 (1976) 1365–1373.
[4] M. Sugano, S. Kanno, T. Satake, Acta Metall. 37 (1989) 1811–1820.
[5] M.R. Bache, W.J. Evans, M. McElhone, Mater. Sci. Eng. A 234-236 (1997) 918–922.
[6] H. Oguma, T. Nakamura, Int. J. Fatigue 50 (2013) 89–93.
[7] F. Yoshinaka, T. Nakamura, K. Takaku, Int. J. Fatigue 91 (2016) 29–38.
[8] T.P. Chapman, K.M. Kareh, M. Knop, T. Connolley, P.D. Lee, M.A. Azeem, D. Rugg, T.C. Lindley, D. Dye, Acta Mater. 99 (2015) 49–62.
[9] F. Yoshinaka, T. Nakamura, S. Nakayama, D. Shiozawa, Y. Nakai, K. Uesugi, Int. J. Fatigue 93 (2016) 397–405.
[10] I. Serrano-Munoz, J.-Y. Buffiere, R. Mokso, C. Verdu, Y. Nadot, Sci. Rep. 7 (2017) 45239.
[11] T. Ikeda, T. Umetani, N. Kai, M. Endo, T. Matsuo, K. Ogi, JFS 89 (2017) 570–576.
[12] I. Serrano-Munoz, J.Y. Buffiere, C. Verdu, Y. Gaillard, P. Mu, Y. Nadot, Int. J. Fatigue 82 (2016) 361–370.
[13] A. Kumar, C.J. Torbet, J.W. Jones, T.M. Pollock, J. Appl. Phys. 106 (2009) 024904.
[14] A. Weck, T. Crawford, A. Borowiec, D. Wilkinson, J. Preston, Appl. Phys. A 86 (2007) 55–61.
[15] Y. Dong, X. He, Y. Li, Int. J. Fatigue 117 (2018) 63–74.
[16] D. He, Z. Fu, W. Wang, J. Zhang, Z.A. Munir, P. Liu, Mater. Sci. Eng. A 535 (2012) 182–188.
[17] J.-Y. Buffiere, E. Maire, J. Adrien, J.-P. Masse, E. Boller, Exp. Mech. 50 (2010) 289–305.
[18] B.L. Boyce, R.O. Ritchie, Eng. Fract. Mech. 68 (2001) 129–147.
[19] J. Everaerts, B. Verlinden, M. Wevers, Proc. Struct. Integr. 2 (2016) 1055–1062.
[20] S. Chilingaryan, A. Mirone, A. Hammersley, C. Ferrero, L. Helfen, A. Kopmann, T. d. S. Rolo, P. Vagovic, IEEE Trans. Nucl. Sci. 58 (2011) 1447–1455.
[21] M. Vogelgesang, T. Farago, T.F. Morgeneyer, L. Helfen, T. dos Santos Rolo, A. Myagotin, T. Baumbach, J. Synchrotron Radiat. 23 (2016) 1254–1263.
[22] Y. Murakami, S. Kodama, S. Konuma, Int. J. Fatigue 11 (1989) 291–298.
[23] M. Dechamps, P. Lehr, J. Less Common Met. 56 (1977) 193–207.
[24] D. David, E.A. Garcia, X. Lucas, G. Beranger, J. Less Common Met. 65 (1979) 51–69.
[25] H. Guleryuz, H. Cimenoglu, J. Alloys Compd. 472 (2009) 241–246.
[26] V. Sinha, J.M. Larsen, Metall. Mater. Trans. A 43 (2012) 3433–3441.
[27] R.C. McClung, B.H. Lawless, M. Gorelik, C. Date, Y. Gill, R.S. Piascik, in: R.R. Boyer, D. Eylon, G. Lütjering (Eds.), Fatigue Behavior of Titanium Alloys, Warrendale. 1999, pp. 211–218.